

## EFFECT OF WELD HEAT INPUT ON THE MECHANICAL CHARACTERISTICS OF Cr-Mo STEEL BARS USING THE MIG WELDING PROCEDURE

Reuben Adebare ADEWUYI<sup>1,\*</sup>, Oluwasayo Dorcas OLAKOLEGAN<sup>1</sup>,  
Emanuel Abiodun AKEJU<sup>1</sup>

<sup>1</sup>Department of Mechanical Engineering, The Federal Polytechnic, Ado-Ekiti, Nigeria.

### Abstract

*The impact of weld heat input on the mechanical characteristics of this steel was investigated in this study. The weld sample was an ASTM A304 grade A Flat Bar with a thickness of 5.00 millimetres. With the use of a data logger, a K-type thermocouple was installed in the drilled holes to measure the temperature fields at each of the places throughout the welding operation. The welding sample was created by varying three process parameters in the MIG welding process. Welding current, weld passes, and point of interest thermocouple position away from the weld centreline are the parameters. The experiment was designed using Taguchi's L9 orthogonal array to limit the number of experimental runs (DOE). To study the influence of weld heat input, the samples were subjected to mechanical and microstructure testing. The hardness test revealed that when the weld pass on the weld zone, HAZ, and base metal increases, the hardness value falls. The tensile test finding indicated that the tensile strength of samples 80A and 100A rises as the weld pass increases, however sample 60A decreases as the weld pass increases. The impact resistance increased when the weld pass was increased, according to the findings of the impact tests. The distance away from the weld centreline of the region subjected to a certain peak temperature increases as weld heat input increases, according to the weld thermal cycle. The value of the temperature fields increases dramatically as the heat source passes through the specific cross-section, where thermocouples are positioned. Later on, the temperature begins to drop at a slower rate. It's also obvious that when the distance between the measurement point and the weld centreline grows, the temperature drops.*

**Keywords:** *Weldment, Weld thermal cycle, Mechanical properties, Microstructure*

### Introduction

In Nigeria, Materials and Production Technology is the key to optimizing Research, Design, and Construction. Chrome-molybdenum alloy steel [or chrome moly] is a high-pressure, high-temperature alloy. Because of its corrosion resistance and high temperature and tensile strength, it is utilized in the oil and gas, energy, construction, and automotive sectors [1, 2]. The qualities of the alloy make it useful in manufacturing and building. Creep strength, hardenability, wear resistance, stiffness, high impact resistance, and simplicity of manufacture are some of these qualities [2]. The choice of optimal welding factors is one of the most challenging difficulties faced by the fabrication industry. In order to consistently generate high-quality welds in stainless steel and other weldable engineering [metallic] materials, a thorough understanding of the microstructural changes that occur inside the material [weldment] as well as the material's mechanical characteristics is required [2,3].

Steel is the most frequently utilized metallic substance in the world for a variety of uses. This is due to its ductility, tensile strength, hardness, and toughness.

\*Corresponding author: reuben1178@yahoo.com, adewuyi\_ra@fedpolyado.edu.ng +2348038458613

Stainless steel is a durable material. A304 steel bar is a form of stainless steel grading system (ASTM Grading System). A304 stainless steel is also known as 1.4301 stainless steel. The most versatile and extensively used stainless steel is Type 304. It is still sometimes referred to by its former moniker, 18/8, which comes from the nominal composition of type 304, which is 18% chromium and 8% nickel. Type 304 stainless steel is an austenitic stainless steel that may be deep drawn to extreme depths. As a result of this feature, A304 has become the most popular grade for sinks and saucepans. For increased weldability, Type 304 is employed in heavy gauge components [3]. The microstructure has a big impact on the weld characteristics, and the welding process has a big impact on the microstructure as well [3, 4]. Welding involves bringing the surface of the metal to be joined close enough together for atomic bonding to occur as a natural consequence of atomic seeking to create a stable electron configuration for themselves, and the service performance of the welded structure is usually limited by failure initiation within the coarse grain region adjacent to the weld metal, and welding involves bringing the surface of the metal to be joined close enough together for atomic bonding to occur as a natural consequence of atomic seeking to create a stable electron configuration for [5]. Welding, in general, refers to any method that joins materials by attracting inter-molecular interactions rather than solely macroscopic or microscopic mechanical interlocking forces.

Because of its advantages over alternative joining methods, such as design freedom, cost savings, overall weight reduction, and structural performance enhancement, welding has become a common mechanical joining approach in a variety of sectors [5, 6].

Metal inert gas welding is the form of welding employed in this project. Metal Inert Gas [MIG] welding is an arc welding procedure that employs a welding gun to heat and feed a continuous solid wire electrode into the weld pool. A connection is formed by melting the two basic materials together. Along with the electrode, the cannon feeds a shielding gas to assist protect the weld pool from impurities in the air.

Mechanical qualities are crucial weldment features that must meet the application feasibility as well as the welded joint's functioning criteria. Hardness, impact strength [toughness], yield strength, ultimate tensile strength, percentage of elongation, wear resistance, corrosion resistance, and other properties are among them [7,8]. These mechanical qualities are heavily influenced by weld microstructure, which is influenced by cooling conditions, base metal composition, wire electrode composition, and flux composition. Welding process parameters also have a direct/indirect impact on the mechanical characteristics and microstructure of the weld [9, 10]. It is critical to utilize an appropriate welding method under regulated welding variables in order to create a high-quality weld. As a result, the focus of this study is on the microstructural features and mechanical behavior of stainless steel that has been welded utilizing the MIG technique [15, 16].

## Materials

This article looked at the mechanical characteristics of Cr-Mo steel bars with a typical thickness of 5mm. The stainless steel (Cr-Mo) flat bar served as the study's foundation. Other materials utilized in the experiment include a MIG welding equipment, a data-logger with type K thermocouples –3 channel–LU-MTM-380SD, and an electrode (welding coil). Table 1 shows the chemical makeup of the substance in detail.

**Table 1.** Chemical composition of ASTM A304 grade A steel

| C        | Mn      | Si       | P        | S        | Cr          | Ni         | N        |
|----------|---------|----------|----------|----------|-------------|------------|----------|
| 0.0-0.07 | 0.0-2.0 | 0.0-1.00 | 0.0-0.05 | 0.0-0.03 | 17.50-19.50 | 8.00-10.50 | 0.0-0.11 |

The material was welded using the MIG Welding process, and the welding joint used is Double V joint using welding currents of 60, 80, 100 amperes and thermocouple was placed at

distances of 8, 10, 12 respectively away from the weld centreline to study temperature fields of the welded zone (Fig. 1). The welding voltage was constant. The welding passes up to 3 times and the electrode (welding coil) diameter was 2.00 mm.

## Design of Experiment

The goal of the experiment is to find the best welding conditions. The primary impacts and influence of the elements that affect the hardness and tensile strength of the materials were studied using a Taguchi's L9 orthogonal array experimental design. The welding variables to be investigated in this study are classified into two categories: variable factors (given in Table 2) and constant factors (material thickness of 5 mm and electrode diameter of 2 mm). The experimental variables elements of the design are shown in Table 2.

**Table 2.** The experiment variable factors

| Parameters  | Level 1 | Level 2 | Level 3 |
|---|---------|---------|---------|
| Welding Current (A)                                     | 60      | 80      | 100     |
| Weld pass   | 1       | 2       | 3       |
| Thermocouple placement point away from weld points (mm) | 8       | 10      | 12      |

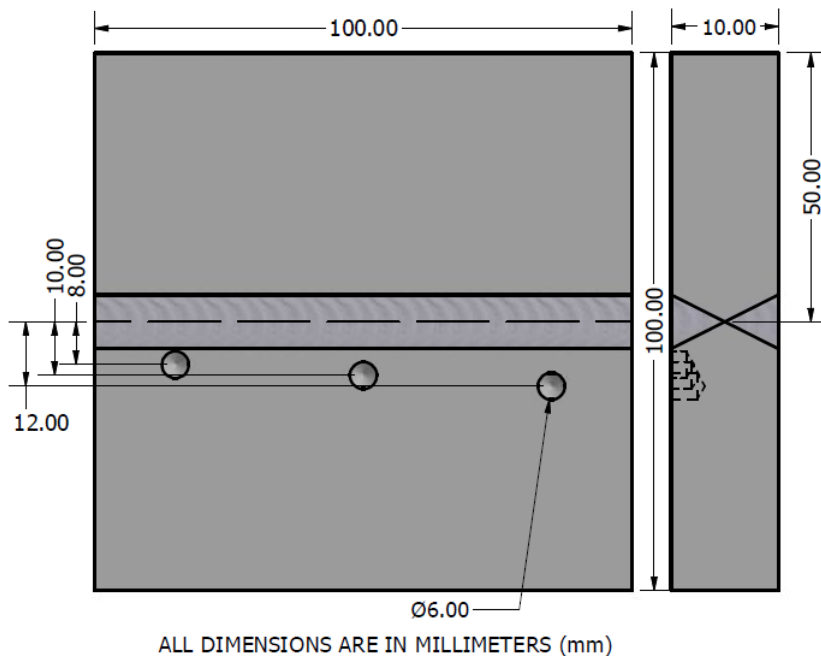


**Fig. 1.** Specimen Design with Autodesk Inventor 2017

The L9 orthogonal array of Taguchi was used to limit the number of experimental runs. Taguchi's L9 (34) orthogonal array, which consists of 9 sets of coded conditions, was used to create the design matrix. The Orthogonal Array for L9 (34) Taguchi's Design is shown in Table 3.

**Table 3.** Orthogonal Array for L9 (3<sup>4</sup>) Taguchi's Design

| Exp No | Welding Current (A) | Weld Pass | Thermocouple placement point |
|--------|---------------------|-----------|------------------------------|
| 1      | 60                  | 1         | 8,10,12                      |
| 2      | 60                  | 2         | 8,10,12                      |
| 3      | 80                  | 1         | 8,10,12                      |
| 4      | 80                  | 2         | 8,10,12                      |
| 5      | 100                 | 1         | 8,10,12                      |
| 6      | 100                 | 2         | 8,10,12                      |

## Results and Discussions

### Weld thermal cycle

Based on the welding parameters selected, the results of the welding temperature field or weld thermal cycle recorded using Data-logger with type K thermocouples –3 channel–LU-MTM-380SD were examined graphically. The Arc welding temperature (1350 - 1450 0C) was recorded with an Ametek Land Cyclops 100L S/N 240671 91 Digital Infrared Thermometer.

Temperature distributions in specimens 60A 1P, 60A 2P, 80A 1P, 80A 2P, 100A 1P, and 100A 2P (see Table 3) throughout the welding process, as shown in Figures (2 to 9). These depict the temperature distributions or weld thermal cycle on the two sides at three points of interest during the first and second weld passes. The heat from the weld is transmitted to the steel bar's edges.

Each specimen's peak Arc welding temperature drops to around T1: 600°C (5500s), 700°C (5535s), 708°C (5610s), 710°C (4923s), 708°C (1021s), 705°C (4650s); T2: 547°C (2776s), 581°C (2840s), 585°C (2890s), 578°C (2430s), 680°C (1585s), 687°C (9750s) and T3: 587°C (3458s), 600°C (5535s), 600°C (5610s), 600°C (4912s), 610°C (995s), 600°C (4750s) for specimens 60A 1P, 60A 2P, 80A 1P, 80A 2P, 100A 1P and 100A 2P respectively. The heat input reaches the edges of the steel bar when the temperature continuously reduces for each of the specimens respectively, due to the effect of air cooling. Because of differences in heat transfer conditions for various weld thermal cycles, weld geometry parameters such as weld current and weld pass impact the heating rate, peak temperature, soaking time, and cooling rate for a particular rate of heat input (welding conditions) (Singh & Mittal, 2017). In general, the weld thermal cycle shown in Figs. 2 to 7 indicates that as the distance between the site of interest and the weld centerline increases:

- lowers the peak temperature;
- after reaching the peak rate temperature, reduces the rate of heating and cooling;
- extend the time it takes to reach peak temperature;
- as time passes, the pace of cooling slows. A decrease in heat input makes the steeper distribution of peak temperature;
- an increase in heat input increases the distance away from the weld centreline of the area subjected to a specific peak temperature;
- preheat condition, increases the soaking time at high temperature and decreases the cooling rate;
- heat input, increasing preheat, decreases the cooling rate but does not affect the soaking time appreciably.

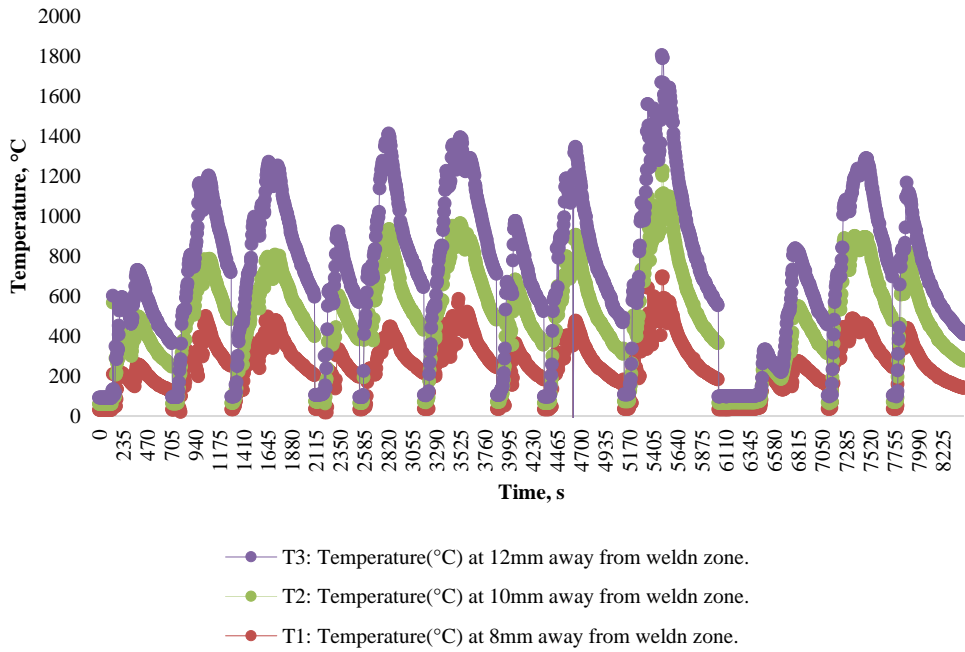


Fig. 2. Thermal Cycle for 60A 1P

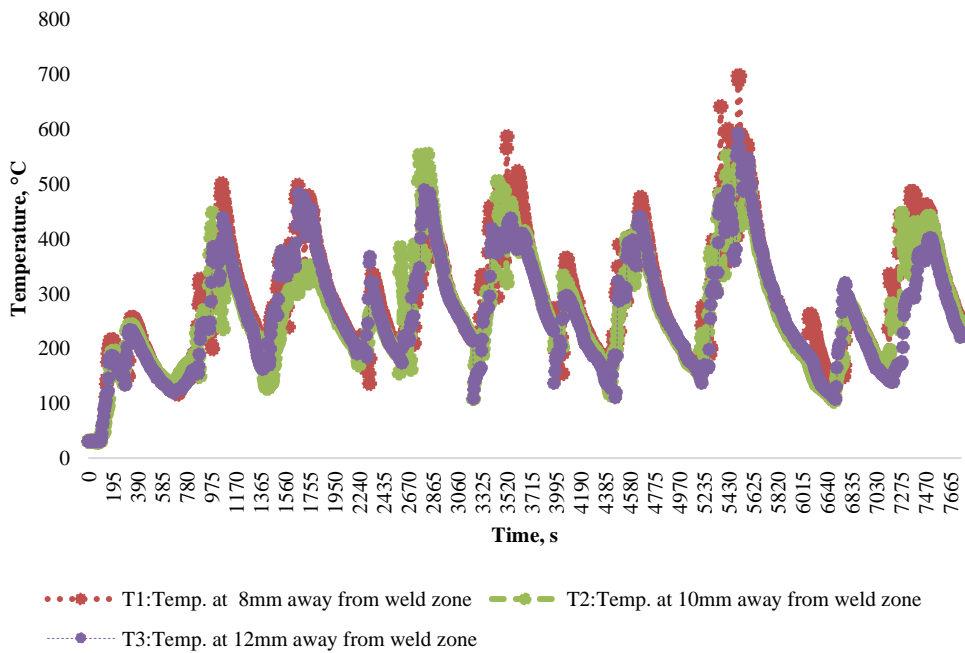


Fig. 3. Thermal Cycle for 60A 2P

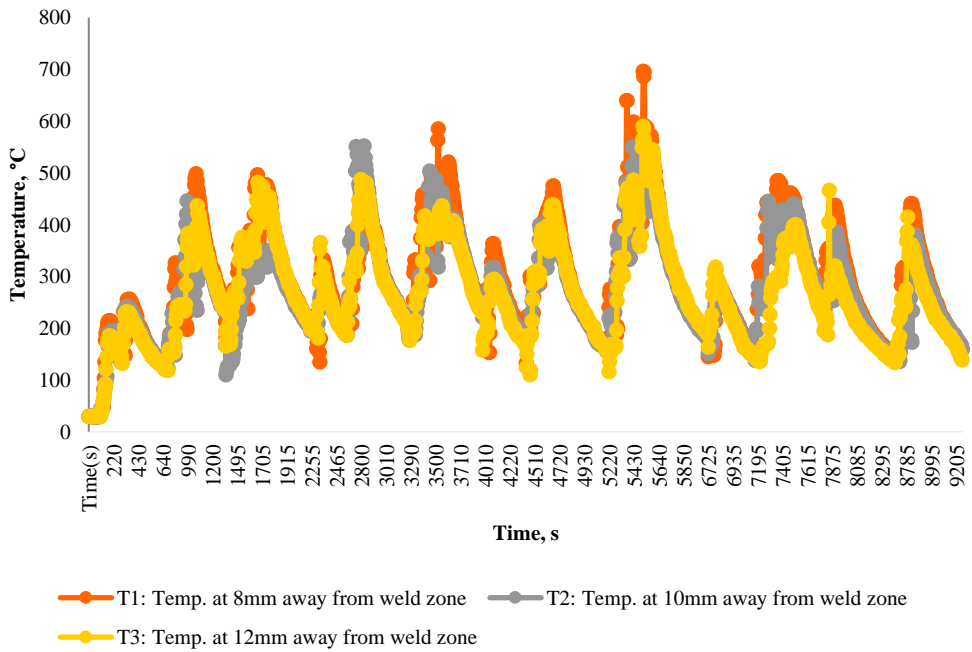


Fig. 4. Thermal Cycle for 80A 1P

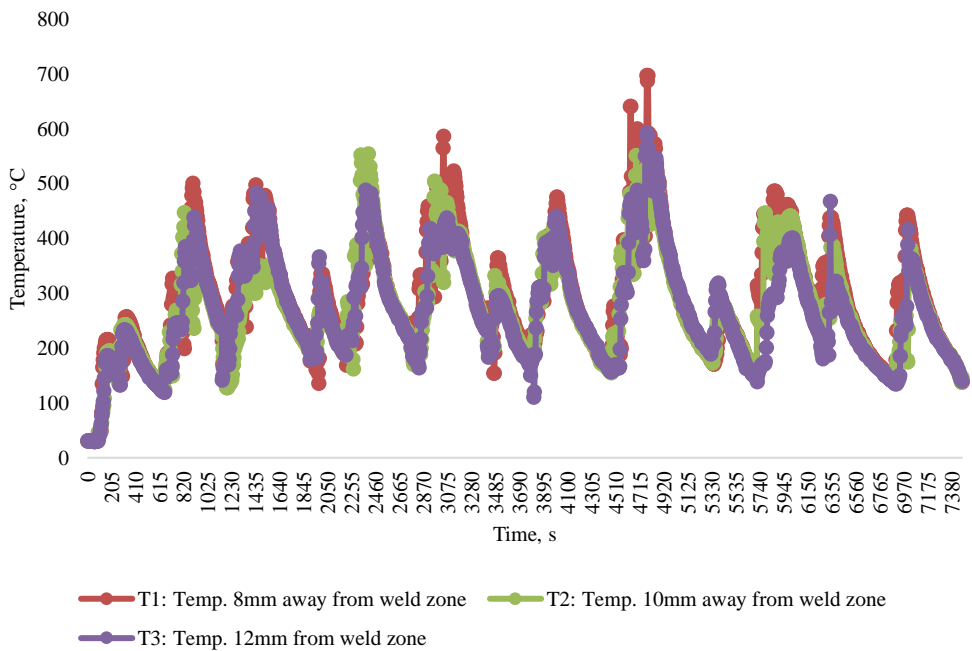


Fig. 5. Thermal Cycle for 80A 2P

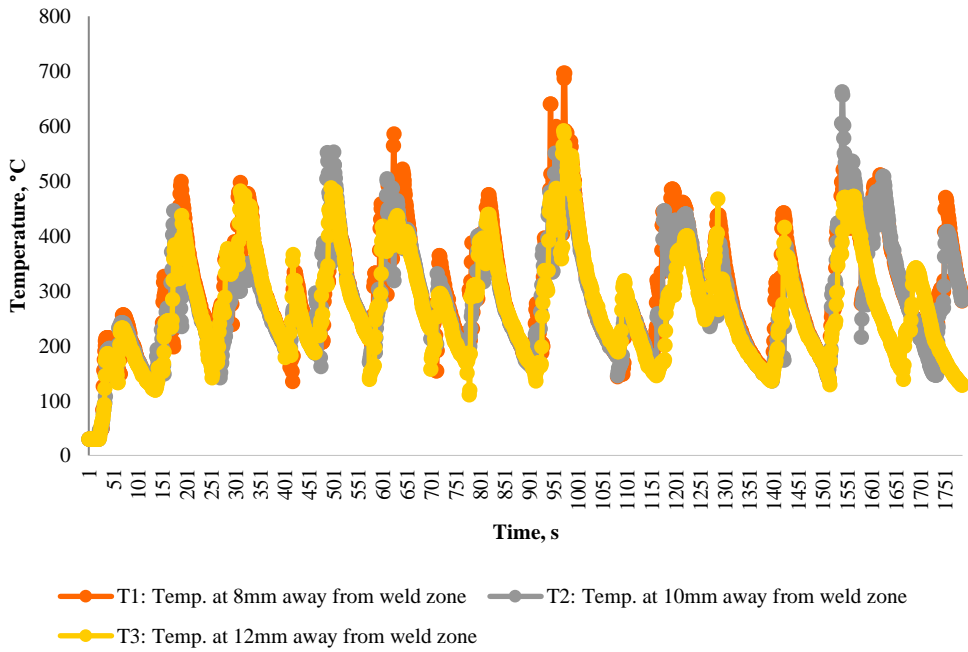


Fig. 6. Thermal Cycle for 100A 1P

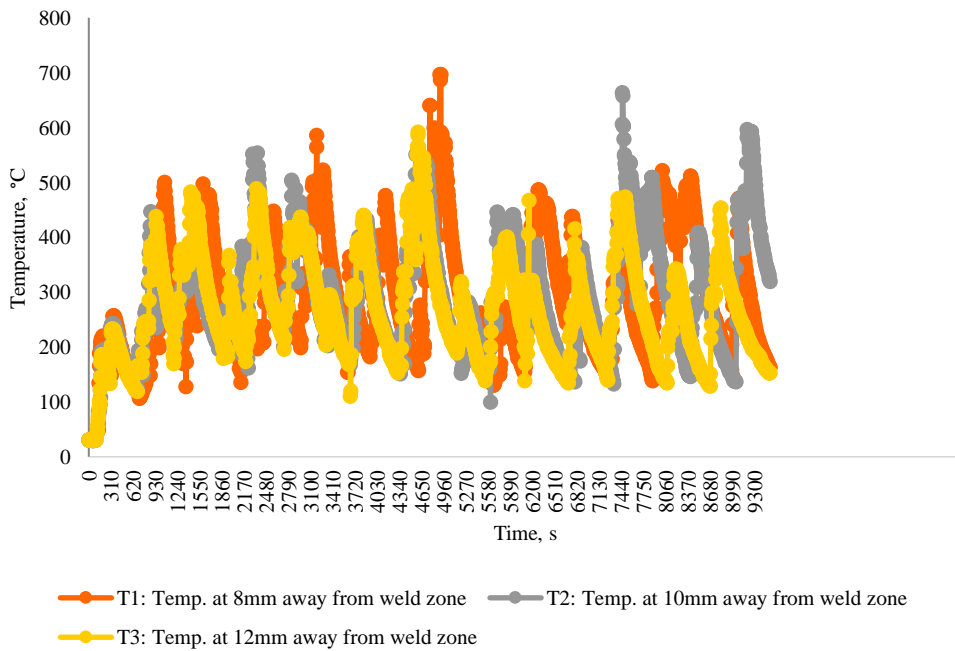
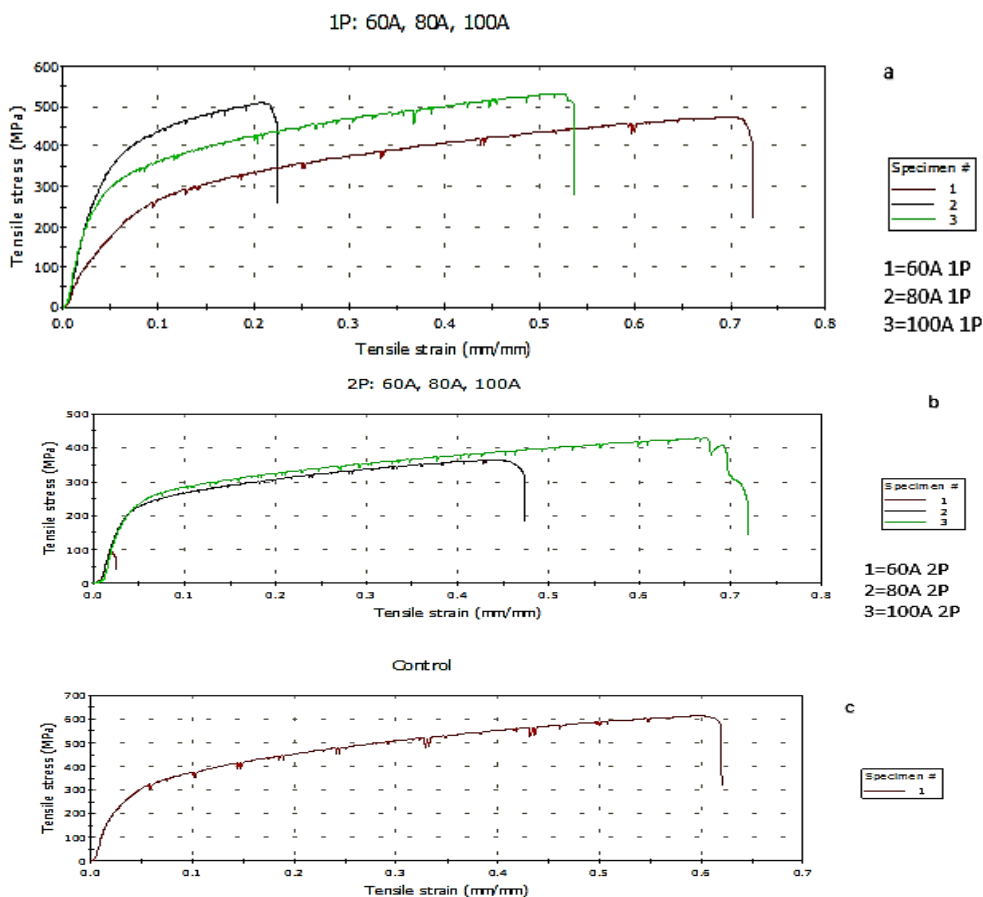


Fig. 7. Thermal Cycle for 100A 2P

### Tensile behaviour of the weldments

The tensile property of the weldments 60A 1P, 60A 2P, 80A 1P, 80A 2P, 100A 1P and 100A 2P is presented in Fig. 8.



**Fig. 8.** Tensile test for 60A 1P, 60A 2P, 80A 1P, 80A 2P, 100A 1P, 100A 2P and Control

From Figure 8a it was observed that the materials deformation changes as the applied forces increased. The test sample 60A 1P shows the highest deformation (0.70062mm) followed by the test sample 100A 1P (0.52292mm) and the test sample 80A 1P shows the lowest deformation (0.20688mm). The test sample 60A 1P fractures at 368.33208Mpa, the test sample 80A 1P fractures at 355.04181Mpa and the test sample 100A 1P fractures at 495.09250Mpa.

From Figure 8b, it was also observed that the materials deformation changes as the applied forces increases and the test sample 100A 2P shows the highest deformation (0.67250mm) followed by the test sample 80A 2P (0.43375mm) and the test sample 60A 2P shows the lowest deformation (0.02084mm). The test sample 60A 2P fractures at 56.75531Mpa, the test sample 80A 2P fractures at 312.75589Mpa and the test sample 100A 1PX fractures at 236.37239Mpa. From Figure 8c, the control experiment deformation value of 0.59896mm and fractured at 552.45478Mpa.

### Hardness and impact behaviour of the weldments

The properties of the specimens were determined using Brinell Hardness Machine and Hounsfield Balanced Impact machine. The hardness and impact properties of the six samples were

presented in Fig. 9. Four tests were carried out on each sample. From the obtained results, it was observed that sample 60A 2P has the highest impact value (63.24J) and sample 60A 1P has the highest hardness value (147.0HV) as shown in Fig. 10.

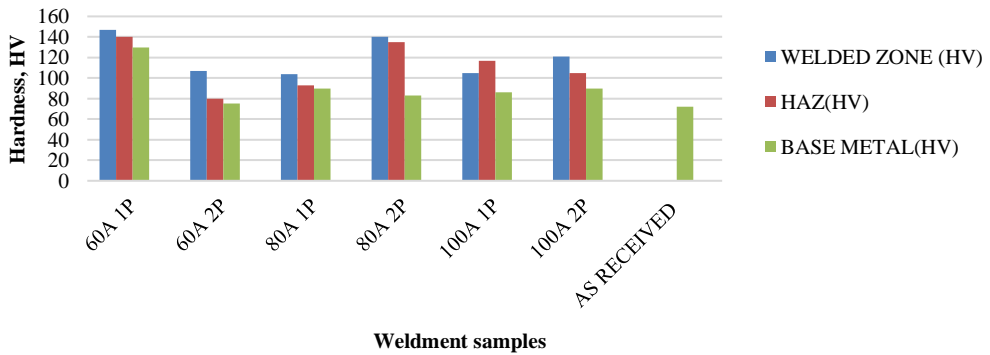


Fig. 9. Hardness distribution on the weldments

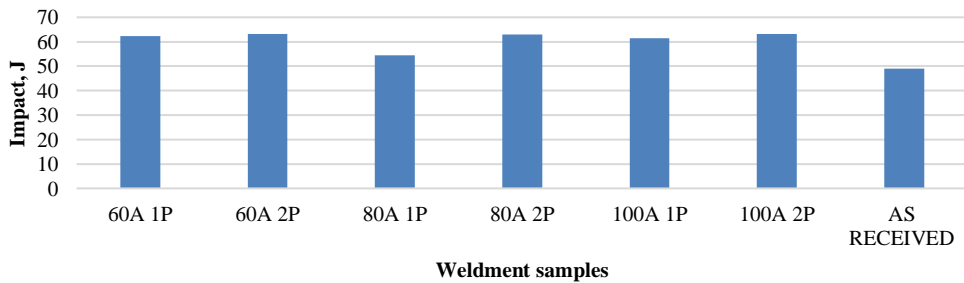


Fig. 10. Impact distribution on the weldments

**Microstructure analysis**

SEM was used for microstructural examination to disclose characteristics of the welded specimens. After the first and second weld passes on each of the specimens, three zones were considered: base metal (BM), weld zone (WZ), and heat-affected zone (HAZ) to analyze the influence of heat input as a function of weld thermal cycle, which led to the varied microstructure of each weldment.



Fig. 11. The microstructural results for 60A 1P at BM, WZ and HAZ

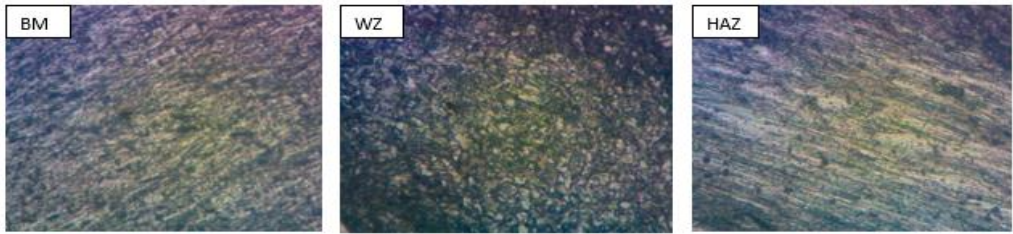


**Fig. 12.** The microstructural results for 60A 2P at BM, WZ and HAZ



**Fig. 13.** The microstructural results for 80A 1P at BM, WZ and HAZ



**Fig. 14.** The microstructural results for 80A 2P at BM, WZ and HAZ

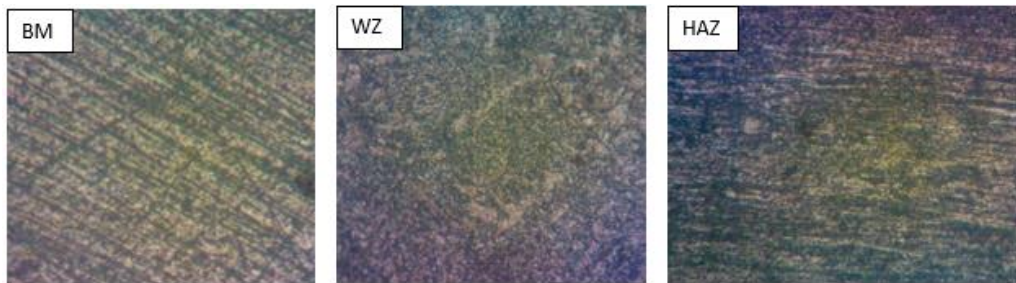


**Fig. 15.** The microstructural results for 100A 1P at BM, WZ and HAZ



Fig. 16. The microstructural results for 100A 2P at BM, WZ and HAZ

Fig. 11 indicates that the base metal's microstructure is mostly ferrite, with a small percentage of pearlite phases. It showed that the metal had a small proportion of carbon, the heat did not affect the feature. The grain boundary is closed. The microstructure of the welded zone consists of pearlite and ferrite. This showed that the metal contains more percentage of carbon. The grain phases are rough and the grain boundaries are closed. The microstructure of the heat-affected zone (HAZ), consists of alpha ferrite and pearlite. The grain phases are fine and the grain boundaries are closed.

Fig. 12 shows the base metal's microstructure, which is made up of alpha ferrite and pearlite. The grain phases are rough. The welded zone consists of pearlite majorly with a small proportion of ferrite. This showed that the metal contained more percentage of carbon. The grain phases are rough. The heat-affected zone (HAZ), consists of alpha ferrite and pearlite and the grain phases are fine.

Fig. 13 presents the microstructure of the base metal, consists of a mixture of alpha ferrite and pearlite and the grain phases are rough with the microstructure of the welded zone, consists of alpha ferrite and pearlite and the grain phases are fine and the microstructure of the heat affect zone (HAZ), consist of alpha ferrite and pearlite with rough grain phases.

Fig. 14 depicts the microstructure of the base metal, which consists of alpha ferrite and pearlite and the grain phases are rough and the grain boundaries are close with the microstructure of the weld zone, which consists majorly pearlite and less ferrite and the grain phases are rough. The microstructure of the heat-affected zone consists majorly of pearlite and a very small proportion of ferrite and the grain phases are fine. This showed that the zone contained more proportion of carbon, which means that heat affects the zone.

Fig. 15 and Fig. 16 presents the microstructure of the base metal, it consists of alpha ferrite and pearlite and the grain phases is fine, and the microstructure of the welded zone, consists of alpha ferrite and pearlite and the grain phases are fine. The microstructure of the heat-affected zone (HAZ) consists of a mixture of pearlite and ferrite and the grain phases are fine.

## Conclusions

The hardness of the samples was found to decrease as the weld pass at the weld zone, HAZ, and base metal increased. The tensile characteristics of 80A and 100A were found to rise when the weld pass was increased, but the tensile values of 60A decreased as the weld pass was increased. The impact property of the samples was found to increase when the weld pass was increased. The cooling ratio is likewise gradually decreasing, resulting in a stable microstructure change.

## References

- [1] Adewuyi R. A., and Aweda J.O., *Characterization of weld heat input effects on Mechanical Properties of Cr-Mo Steel bar using TIG welding process*, **European Journal of Materials Science and Engineering** 2021, 6(4), pp 192-204, doi: 10.36868/ejmse.2021.06.04.192.

- [2] Adewuyi R. A., and Aweda J.O., (2021), *Modeling and simulation of welding temperature fields in Cr-Mo steel bar*, **European Journal of Materials Science and Engineering**, 2021, 6(1), pp. 3-18, doi: 10.36868/ejmse.2021.06.01.003.
- [3] Hansen, J. L. *Numerical Modelling of Welding Induced Stresses*. The Technical University of Denmark, Department of Manufacturing Engineering and Management. Denmark: Department of Manufacturing Engineering and Management, Technical University of Denmark, 2003.
- [4] Hemaid, A., Tawfeek, T., & Gaheen, O. A. *An Investigation into Effect of Butt Welding Parameters on Weldment Mechanical Properties*, **American Journal of Mechanical Engineering**, 2016, 4(3), pp. 92-98.
- [5] Jeyaprakash, N., Adisu, H., & Arunprasath, M. *The Parameters and Equipment Used in TIG Welding: A Review*, **The International Journal Of Engineering And Science**, 2016, 4(2), pp. 11-20.
- [6] Kaiser, M. S. *Effect of Heat Input on the Weld Metal Toughness of Chromium-Molybdenum Steel*, **International Scholarly and Scientific Research & Innovation**, 2013, 1(7), pp. 33-35.
- [7] Monika, K., Bala, M., Nanda, P., Prahalada, K., *Effect of Heat Input on the Mechanical Properties of MIG Welded Dissimilar Joints*, **International Journal of Engineering Research & Technology**, 2013, 2(9), pp. 142-153.
- [8] Muratoglu, M., Eroglu, M. *Effect of molybdenum on the intercritical heat-affected zone of the low carbon Cr-Mo steel*, **Asian Transaction on Engineering**, 2011, 1(4), pp. 1-5.
- [9] Amraei, M., Ahola, A., Afkhami, S., Björk, T., Heidarpour, A., & Zhao, X. L. Effects of heat input on the mechanical properties of butt-welded high and ultra-high-strength steels. **Engineering Structures**, 2019, 198(06), 109460, doi:10.1016/j.engstruct.2019.109460.
- [10] Naik, A. B. *Effect of Process Parameters of Tungsten Inert Gas Welding on Welding of Duplex Stainless Steels*, **International Journal for Research in Applied Science and Engineering Technology**, 2018, 6(1), pp. 2818–2827, doi: 10.22214/ijraset.2018.1388.
- [11] Nirmalendhu, C., Ramesh, R., Asish, B. *Design optimization of Process Parameters for TIG Welding based on the Taguchi Method*, **International Journal of Current Engineering and Technology**, 2014, 2, pp. 12-16.
- [12] Odebiyi, O., Oseni, G., & Adedayo, S. *Effect of parallel heating on properties of a welded AISI 8438 Steel*, **International Journal of Engineering**, 2013, XI(3), 233-236.
- [13] Pawaria, N., Kataria, S., Goyal, A., Sharma, S. *Effect of Heat Input and Shielding Gas on Hardness, Tensile and Impact Strength of 2.25 Cr-Mo Steel Weld Metals in GMAW*, **International Journal of Research in Mechanical Engineering & Technology**, 2013, 3 (2), pp. 266-269.
- [14] Prashant, K. S., Pankaj, K., Baljeet, S., & Rahul, K. S. *A review on TIG welding for optimizing process parameters on dissimilar joints*, **Journal of Engineering Research and Applications**, 2015, 5 (2), pp. 125-128.
- [15] Sadiq, Y. A. *Study the Effect of Welding Joint Location on the Fatigue Strength and Fatigue Life for Steel Weldment*, **Asian Transactions on Engineering**, 2012, 2(4), pp. 1-13.
- [16] Xiaowei, P., Zhang, C., SuoLi, Deng, D. *Simulating welding residual stress and deformation in a multi-pass butt-welded joint considering balance between computing time and prediction accuracy*, **The International Journal of Advanced Manufacturing Technology**, 2017, 93, pp. 2215–2226. DOI 10.1007/s00170-017-0691-5.
- [17] Xiang, J., Chen, F. F., Park, H., Murphy, A. B. *Effects of Diffusion of Metal Vapour in an Argon TIG Welding Plasma*, **Korea: CSIRO Manufacturing**, (2018).

Received: January 04, 2022

Accepted: February 11, 2022